Chapter 3

Gaussian-to-Lévy statistical crossover in dye-scatterer random amplifying media: Monte Carlo simulation

3.1 Motivation

In the previous chapter we showed by theoretical analysis and experiments, that for very high gain (small l_g) and strong scattering (low l_t) characterizing the RAM, the fluctuations of intensity follow Lévy statistics where a few large events dominate the intensity. In this chapter, we present a Monte Carlo simulation of photon diffusion in a RAM where the paths of the spontaneously emitted photons performing random walks within the gain medium are traced up until the photons finally exit the RAM. From this we estimate the emission intensities and their statistics for various choice of parameters characterizing the RAM. We find in these simulations, large random fluctuations in the emission intensity that exhibit Lévy-statistical features when the scattering is strong and the gain high, consistent with our experimental observations and our theoretical analysis.

Here, we emphasize that these simulations supplement our work (discussed in chapter 2), in that they provide a means of studying the crossover from the Gaussian to the Lévy statistics by systematically varying the various parameters in the problem over regions of

the parameter space not readily accessible in physical experiments. These include small values of the gain length (l_g) corresponding to large pumping or high dye concentration. In the latter case, in experiments, the suspensions became unstable as particles coagulated and sedimented. Further, varying the refractive index mismatch (δn) over a wide range proved difficult in practice, as it needed solvents that had the required refractive index and could dissolve the dye, and in which the particles remain uniformly suspended without coagulation. In the Monte Carlo simulation, on the other hand, altering δn posed no problem at all and it was continuously varied. Further, a continuous range of particle sizes (d) and number densities (n_s) could be easily considered in our simulation providing a continuous range of transport mean free paths (l_t). Thus, Monte Carlo simulations, unlike experiments, permit us vary continuously parameters like transport mean free path (l_t), gain length (l_g) and refractive index mismatch (δn).

The connection between the present simulation and our earlier work (discussed in chapter 2) calls for some clarification. In both cases, we are considering an ensemble of different realizations of the randomness, but with a difference. In the case of the physical experiment, we obtain the different microscopic realizations of the bulk RAM by considering different configurations of the scatterers. This is readily obtained in our experiments for the case of a dye-scatterer system, where the random scatterers (undergoing constant Brownian motion) move diffusively and thus explore the different complexions (over a time scale which is, of course, much longer than the transit time of light through the sample, but shorter than the interval between successive pump pulses). Thus, each pump pulse samples essentially a different static realization of the RAM. These correspond to randomly varying the structure factor for the scattering system over the ensemble of possible structure factors. In the present simulation, however, the randomness is realized effectively by the random choice of the initial position and direction of spontaneous emission of the seed photon and its subsequent probabilistic scatterings. From the simulation results (which will be discussed in the later sections), it is quite evident that the statistics of the emitted intensity in the two cases above (namely our earlier experiments and the present simulations) show qualitatively the same behaviour as function of the gain and the strength of scattering. This strongly suggests that

these two random realizations are related through a kind of ergodicity. It is to be noted, however, that the present simulation corresponds literally to our analytical treatment of photon diffusion in a RAM (section 2.2).

In the following section, we discuss the Monte Carlo simulations of random walk of photon in a dye-scatterer RAM[1].

3.2 Monte Carlo simulation

The Monte Carlo simulation considered elastic multiple scattering of light due to scatterers suspended randomly in an amplifying continuum (RAM). Stated in terms of a photon (pencil of light), physically, this leads to a diffusive motion (all interference effects giving possible localization, weak or strong, are totally neglected) and concomitant amplification of a spontaneous photon. In our simulation, this diffusive motion was viewed as a random walk of the photon where the step lengths and the step directions are uncorrelated and followed a prescribed probability distribution. The stimulated amplification (in the active medium) was introduced through an exponential number growth (multiplicative amplification) of the initial seed photon.

Monte Carlo simulations were performed on a RAM consisting of bulk active (amplifying) liquid medium with passive point-like scatterers suspended randomly in it. The sample was assumed to be contained in a cubic cell (side $L = 1$ cm) and uniformly pumped. We first performed Monte Carlo simulations for parameters l_t, l_g and δn, corresponding to our earlier experiments on dye-scatterer RAMs (consisting of TiO_2 scatterers suspended in Rhodamine 6G and Rhodamine 640 perchlorate dye solutions), so as to validate the simulation technique. On obtaining comparable results, the simulations were later extended to regions of parameter space difficult to access experimentally (e.g. low l_g or l_t).

In the simulation, a spontaneous (seed) photon was assumed emitted at some position (x, y, z) in the active medium with $0 < x/L, y/L, z/L < 1$, picked randomly from a uniform distribution. It travelled along some random direction over a distance l in the active medium

[1] see Appendix B, at the end of the Thesis.

and then underwent scattering event, where the direction of its propagation changes probabilistically. The trajectory of this photon was simulated keeping track of its position (x, y, z) coordinates, the direction of propagation (scattering angle θ and azimuthal angle ϕ), the cumulative length of travel within the active bulk medium, and the number of scatterings it underwent before finally exiting the RAM. More explicitly, the distance l_i travelled by the photon between two successive scattering events, i and $i + 1$, was picked randomly from the exponential probability density for the scattering length

$$P(l_i) = \frac{1}{l_s}\, exp(-\frac{l_i}{l_s}) \tag{3.1}$$

with mean as the scattering mean free path $l_s = 1/n_s\sigma_s$, where, n_s is the scatterer density. σ_s is the scattering cross-section of the individual scatterer (calculated using BHMIE subroutine, [1]). The path length distribution was simulated by

$$l_i = -l_s\, ln\, (random), \tag{3.2}$$

where, *random* is a random number chosen from a uniform distribution over the interval (0,1).

On suffering a scattering event, the photon changed direction with the new scattering angle θ picked randomly from the Henyey-Greenstein [2] probability distribution :

$$P(\theta) = \frac{1 - g^2}{(1 + g^2 - 2gcos\theta)^{3/2}} \tag{3.3}$$

that accounts for the anisotropy in scattering. Here, g is the anisotropy parameter (calculated using BHMIE subroutine, [1]). The azimuthal angles, ϕ, after scattering were uniformly distributed over the range (0 to 2π) as the scattering is cylindrically symmetric around the incident direction. Here, it is to be noted that the angles of scattering were always chosen with respect to the initial direction of propagation of the photon, i.e., defined on a local coordinate frame whose origin was at the position of the photon.

In this fashion, the path of the photon was monitored till it exits the sample, that is, till at least one of its coordinates became less than zero or greater than one. The total emitted intensity ($I(l)$) associated with this photon is then $I(l) = I_o exp(l/l_g)$, where, I_o is the starting

intensity at the first scatterer, and $l = \sum_i l_i$ is the total length of travel of the photon in the active medium. As the photon may exit from any face, the calculated intensity constituted the total emission intensity from all faces. This process of tracing the path of a spontaneously emitted photon within the RAM till it exits was termed as a "simulation run" and was repeated $N \sim 500{,}000$ times. Each run, thus, corresponded to a different probabilistic photon path. These simulated photon paths differed in their total lengths l in the active bulk, thereby giving the observed fluctuations of intensity. The mean intensity was then obtained by summing up the intensities obtained in the various simulation runs (photon paths) and dividing the summed intensity by the total number of such runs.

While it may appear that in our simulation all photons incident from a given direction in a particular scattering event are scattered into the same direction, it is essentially not so because of the probabilistic nature of the scattering considered in our simulation. We now show below that our probabilistic simulation does not imply the highly unphysical bosonic correlation among the photons wherein all the photons in a chosen direction of incidence on a scatterer are scattered into the same direction.

Consider the n-step random walk of a 'seed' photon injected or spontaneously emitted at a random position $\vec{r}_o$ with the random initial direction $(\Omega_o \pm \frac{1}{2}\Delta\Omega)$ of emission chosen randomly. Let, $\vec{r}_1$, $\vec{r}_2$ .... $\vec{r}_n$, be the positions for the n subsequent scattering events. Also, let, $\Omega_1 \pm \Delta\Omega_1/2$, $\Omega_2 \pm \Delta\Omega_2/2$ ....$\Omega_n \pm \Delta\Omega_n/2$, be the n subsequent scattering angles with angular widths $\Delta\Omega_i$. Here, Ω_i stands for the polar angles (θ_i, ϕ_i) corresponding to the i^{th} scattering event. The amplifying medium is introduced here through an exponential gain factor $(e^{\frac{|\vec{r}_i - \vec{r}_{i+1}|}{l_g}})$ in the photon number as it propagates.

As in the simulation of the random walk, the step lengths $|\vec{r}_i - \vec{r}_{i+1}|$ and the scattering directions $(\Omega_i \equiv \theta_i, \phi_i)$ are assumed uncorrelated random variables with specified probability densities. For the chosen given initial condition, the number N_n of photons at the end of the n-step random walk is straightforwardly given by :

$$N_n\{(\Omega_i \pm \Delta\Omega_i/2), (|\vec{r}_i - \vec{r}_{i+1}|)\} = \left(\frac{d\Omega_o}{4\pi}\right) exp\left(\frac{|\vec{r}_1 - \vec{r}_o|}{l_g}\right) \prod_{i=1}^{n} \left(\frac{\sigma(\Omega_i)\Delta\Omega_i}{\sigma_{total}}\right) e^{(|\vec{r}_i - \vec{r}_{i+1}|/l_g)}, \quad (3.4)$$

where, the probability for scattering angles are introduced through the cross-section

$(\sigma(\Omega_i)/\sigma_{total})$, with

$$\sigma_{total} = \int \sigma(\Omega_i)\, d\Omega_i \tag{3.5}$$

Inasmuch as the random variables are uncorrelated, we can now integrate over all the angles (Ω_i) giving

$$\begin{aligned} N_n\{|\vec{r}_i - \vec{r}_{i+1}|\} &= \left\langle \prod_{i=0}^{n} exp\left(\frac{|\vec{r}_i - \vec{r}_{i+1}|}{l_g}\right)\right\rangle \\ &= \left\langle exp\left(\frac{\sum_i |\vec{r}_i - \vec{r}_{i+1}|}{l_g}\right)\right\rangle , \end{aligned} \tag{3.6}$$

where, $\sum_i |\vec{r}_i - \vec{r}_{i+1}|$ is the total path length traversed by the seed photon in its n-step random walk and $< .... >$ denotes average over the random step-lengths assumed to be distributed exponentially with a mean step-length (mean free path) l_s. This is precisely the gain factor being analyzed in our Monte Carlo simulation to determine the intensity fluctuation statistics. Thus, probabilistically our simulation effectively takes into account all possible scattering directions for the individual photons.

Simulations were carried out for a wide range of the RAM parameters. Monodisperse samples with suspended scatterers of diameters 0.18 μm, 0.22 μm, 0.26 μm, 0.30 μm, 0.34 μm and 0.38 μm were considered. Scatterer size being smaller than the wavelength (λ = 0.633 μm), geometrical optics is ruled out. For a suspension of a given particle size (d), scatterer densities (n_s) of 10^{10}/cc to 10^{12}/cc were considered. Keeping the refractive index of scatterers (n_{sphere}) constant= 2.7 (refractive index of TiO_2) and varying the refractive index of the active bulk (n_{bulk}) from 1.3 to 2.6 (in steps of 0.04), the refractive index mismatch ($\delta n = n_{sphere} - n_{bulk}$) between the active bulk and the passive scatterers was varied from 0.1 to 1.4. Increase in both the diameter (d) of the scatterers and the refractive index mismatch (δn) served to increase the scattering strength within the RAM. Further, the simulations were performed for different gain lengths l_g, ranging from 0.2 cm (high gain) to 10.0 cm (low gain), to examine the effect of gain. Thus, by varying both the scattering strength (by δn, d and n_s) and the gain (by l_g), we could examine the synergy between the scattering and the gain in the RAM.

To illustrate the ease with which the RAM parameters could be chosen over a wide range in Monte Carlo simulation (as discussed in section 3.1), we give a few representative values.

For a large particle size of 0.38 μm (λ = 0.633 μm, $n_s = 10^{12}$/cc), the transport mean free path (l_t) ranges from 0.14 cm to 3.73×10^{-4} cm, and the anisotropy parameter (g) ranges from 0.91 to 0.36 corresponding to variation in δn from 0.1 to 1.38. For the smaller particle size considered, (0.18 μm), l_t varied from 1.18 cm to 4.29×10^{-3} cm, and g ranged from 0.72 to 0.45 corresponding to variation in δn from 0.1 to 1.38.

Before we turn to the statistical analysis of the results of our simulations, we would like to clarify a rather subtle point which is crucial to our analysis below. At first sight, the appearance of the product of n ($n \gg 1$) random factors on the right-hand side of equation (3.10) would imply that the product is to be described, strictly speaking, by a lognormal distribution. Now, a lognormal distribution is a narrow, light-tailed distribution for which all the moments are finite (see chapter 1). The point, however, is that while the above is true asymptotically (in the limit $n \to \infty$), it is not relevant when n is small and the standard deviation for the fluctuations is large [3]. In this "intermediate asymptotic limit", the lognormal distribution behaves essentially as a broad, fat-tailed distribution much like the Lévy distribution. More specifically, consider the case $n = 1$. Here, the probability density ($p_g(g)$) for the gain factor $g = e^{L/l_g}$, with L distributed exponentially as $p_L(L) = (1/l_s)e^{-L/l_s}$, gives $p_g(g) = \alpha/g^{1+\alpha}$: α being the Lévy exponent (see chapter 4, section 4.3), which is, of course, the Lévy statistical probability density. More generally, when n is greater than one but not too large, and the dispersion is high, the whole product is still dominated by the occurrence of rare but large factor in the product. This, therefore, still gives a Lévy statistics. It is with this in mind that we will now discuss our Monte Carlo simulation results in terms of a Lévy fit to the statistics.

3.3 Results

We now discuss the results of the simulation. Figures 3.1(a-l) give the mean emission intensity (log scale) as a function of refractive index mismatch (δn) for $n_s = 10^{10}$/cc and λ = 0.633 μm. Each of the twelve frames in this figure correspond to a different value of l_g. Six curves are drawn in each frame. Each curve represents a different sample, which is monodis-

perse but varies in the size of the suspended particles (scatterers). It may be noted that every point on a curve is the average of the intensity obtained after simulating the random walk of 500,000 photons.

Fig. 3.1(a) gives the mean emission intensity (log scale) as a function of refractive index mismatch (δn) for l_g = 10 cm. From the curves it is seen that irrespective of the scatterer size the mean emission intensity increases with the increase in the δn. Further, for a given δn, an increase in particle size d, increases the mean emission intensity. These results, of course, are to be expected and can be interpreted as follows : An increase both in δn and d makes the scattering stronger which leads to enhanced path length (or dwell time) of photons within the bulk active medium, before they finally exit the RAM. Further, as the gain acquired by the photon increases exponentially with its path length (l) within the active bulk ($exp(l/l_g)$), increase in scattering, leads to enhanced light amplification. This confirms that in such RAMs (dye-scatterer systems) made up of active bulk with randomly suspended passive scatterers, enhanced scattering results in larger emission intensities.

Figures 3.1(b)-3.1(l) are similar except that the gain (l_g^{-1}) in the sample is progressively increased by decreasing the gain length l_g from l_g = 5.0 cm in 3.1(b) to l_g = 0.2 cm in 3.1(l). It is seen that as the gain increases (l_g decreases), the mean intensity values increase, as is expected. Evidently, high scattering and large gain in the RAM lead to enhanced light amplification in a RAM.

While the mean intensity is found to increase with the gain and the scattering strength, as expected, a distinct feature is that for extremely high gain (small l_g) and high scattering (small l_t) the increase is not strictly monotonic (see the jagged curves of Figs 3.1(k) and 3.1(l)). Large fluctuations in the mean emission intensity as function of δn are observed in the simulations, even when it is averaged over 500,000 distinct photon paths. To investigate the reason behind these observed fluctuations and to rule out the possibility of these being artefacts of computation, simulation runs were performed for increasing number of photon paths namely, 100, 1,000, 10,000, 100,000 and 1000,000 paths.

Figures 3.2(a-f) give the mean intensity (log scale) as a function of refractive index mismatch (δn), for different gain lengths with scatterer size = 0.18 μm. Each figure contains

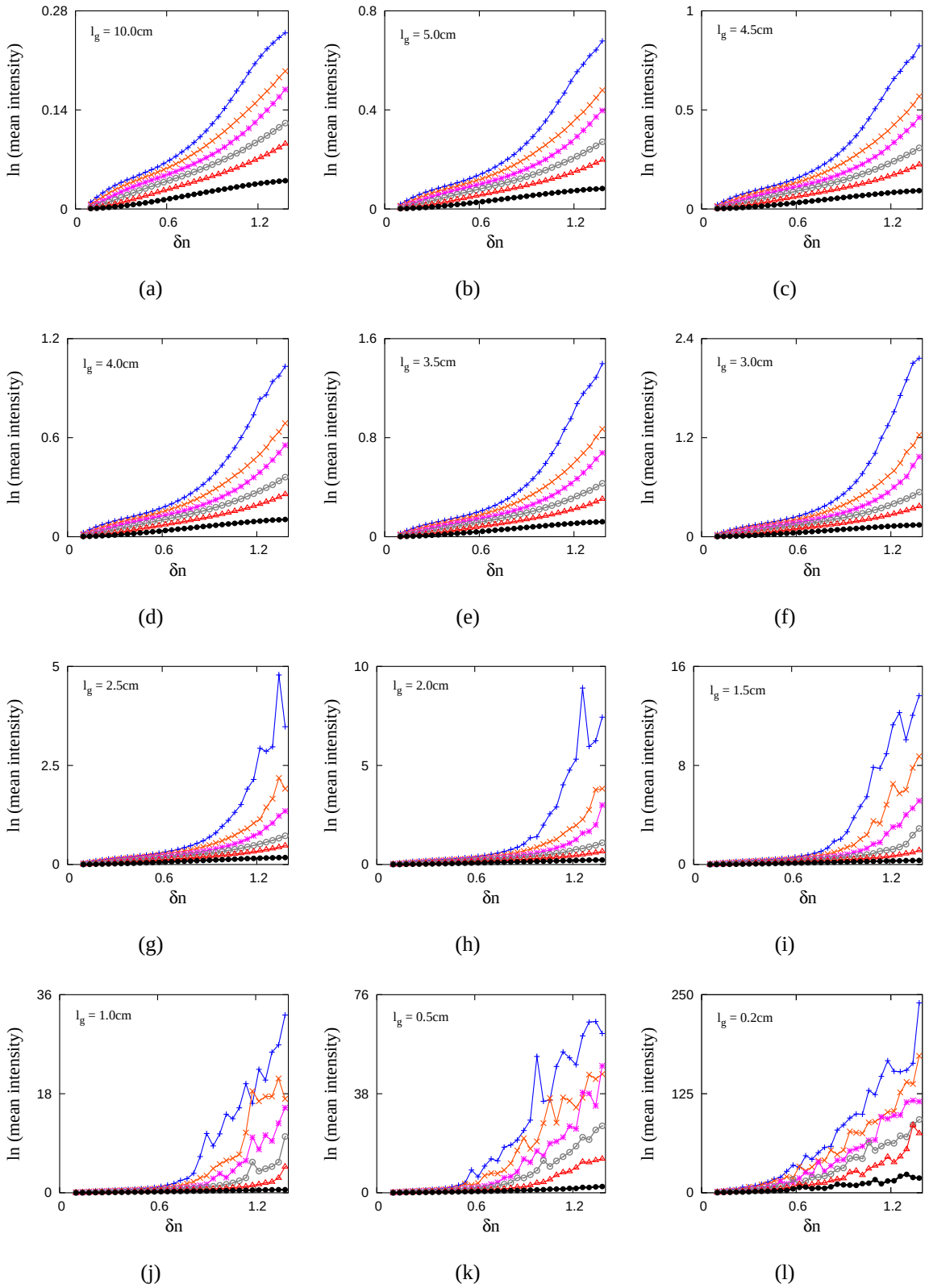

Figure 3.1: *Mean intensity (log scale) as function of δn, with* $n_s = 10^{10}$*/cc ;* • *(black) : 0.18 μm,* △ *(red) : 0.22 μm,* ○ *(gray) : 0.26 μm,* ∗ *(pink) : 0.30 μm,* × *(orange) : 0.34 μm, and* + *(blue) : 0.38 μm, respectively.*

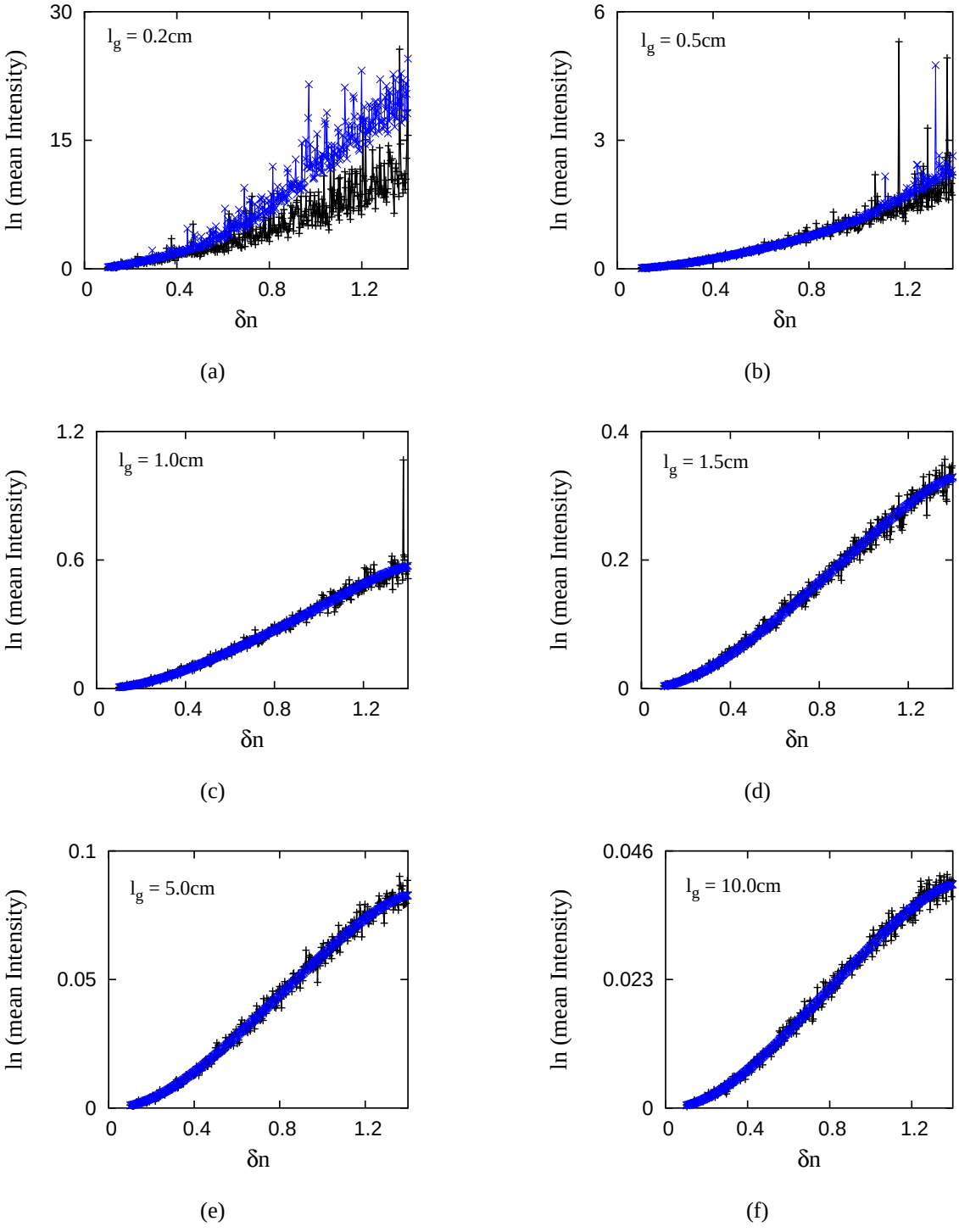

Figure 3.2: *Mean intensity (log scale) as function of δn for various l_g with scatterer size = 0.18 μm; "+" (black): 1,000 simulation runs and "× (blue)" : 1000,000 simulation runs.*

two curves corresponding to simulation runs of 1,000 and 1000,000. Figure 3.2(a) shows the mean intensity as function of δn, for l_g = 0.2 cm (high gain). We notice that despite increasing the number of simulation runs, the large fluctuations in the emission intensity persist; in fact, the fluctuations are more pronounced, implying that it is due to the underlying process taking place inside the RAM, rather than due to inadequate statistics. Further, a positive vertical shift in the mean intensity is observed with the increase in simulation runs, when δn is increased beyond $\sim$ 0.6. The absolute magnitude of this vertical shift increases with the increase in δn. Figures 3.2(b)-(f) show the simulation results for the same system with l_g increased (or the gain decreased) from l_g = 0.5 cm (Fig. 3.2(b)) to l_g = 10.0 cm (Fig. 3.2(f)). We note that, the increase in l_g (or decrease in gain) decreases the mean intensity, as is expected. Further, the figures, clearly, show a reduction in fluctuations in the mean intensity as function of δn, with the increase in simulation runs. In fact, the lesser the gain (high l_g), the greater is the observed reduction in the fluctuations (Fig. 3.2(f)). In addition, we notice that on decreasing the gain, vertical shift in the mean intensity (with δn) for increase in simulation runs is observed at successively higher values of δn and it decreases with the decrease in gain.

To examine the effect of enhanced scattering (due to increased scatterer size) similar simulation study was done on RAM with scatterer size (d) of 0.26 μm (Fig. 3.3) and 0.38 μm (Fig. 3.4). It is clearly seen from figures 3.3(a)-(c) and 3.4(a)-(d) that the fluctuations in the mean intensity as function of δn persist even after increasing the simulation runs from 1,000 to 1000,000. However, these fluctuations gradually die out and the curves become smoother with a decrease in gain (increase in l_g). While for particle size of 0.26 μm, the observed vertical shift in the mean intensity (as function of δn), with increased simulation runs, is noticeable till l_g = 1.0 cm (Fig. 3.3(c)), for larger scatterer size of 0.38 μm (Fig. 3.4(d)), this vertical shift is noticeable for much lower gains (l_g = 1.5 cm).

These simulation results conducted for wide range of parameters characterizing the RAM (i.e. l_g, δn and d), quite conclusively rule out the possibility of the jagged features in the mean emission intensity with δn, seen in the limit of high gain and strong scattering, as arising due to inadequate statistics. We interpret these observations as signature of Lévy statistical

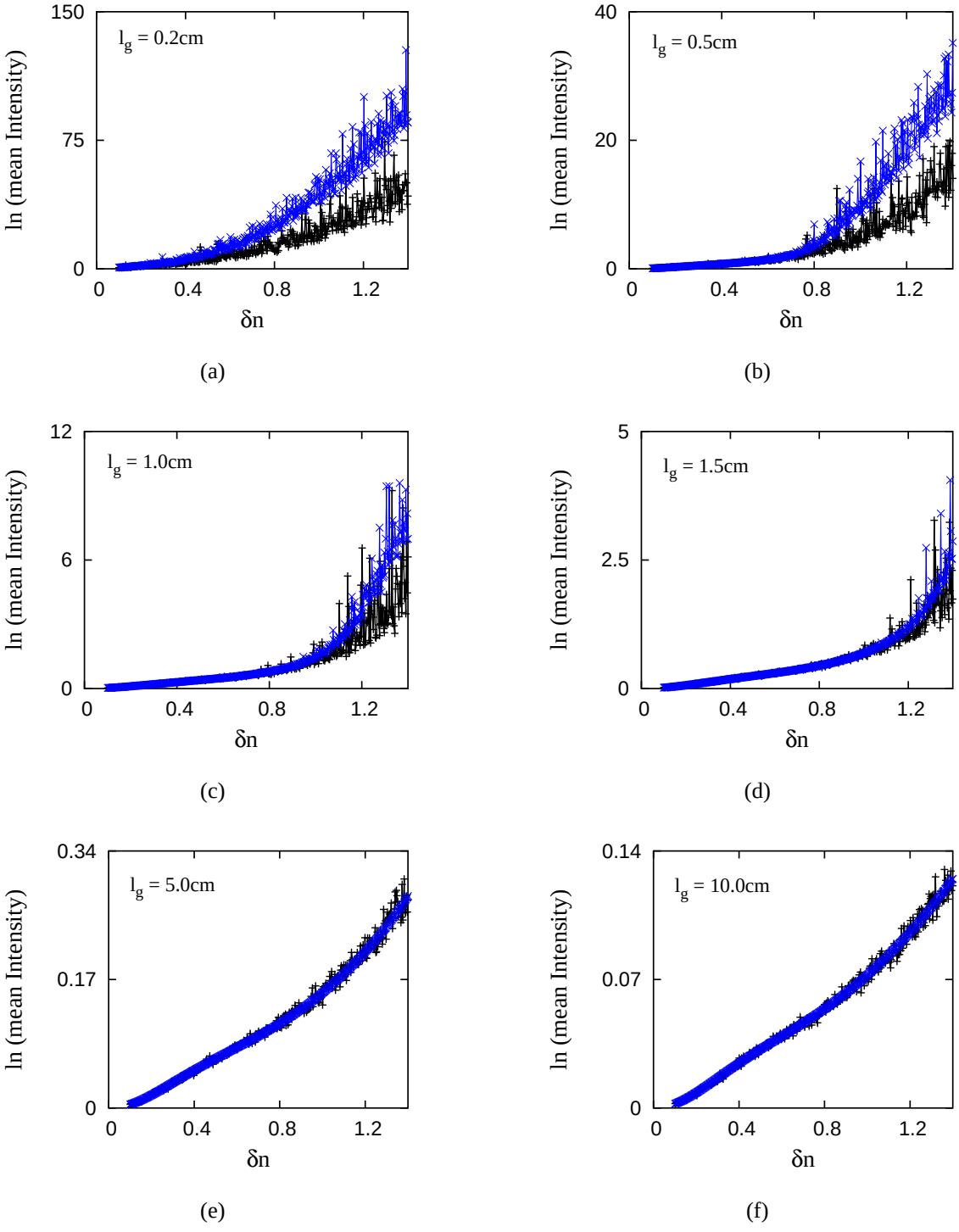

Figure 3.3: *Mean intensity (log scale) as function of δn for various l_g with scatterer size = 0.26 μm; "+" (black): 1,000 simulation runs and "× (blue)" : 1000,000 simulation runs.*

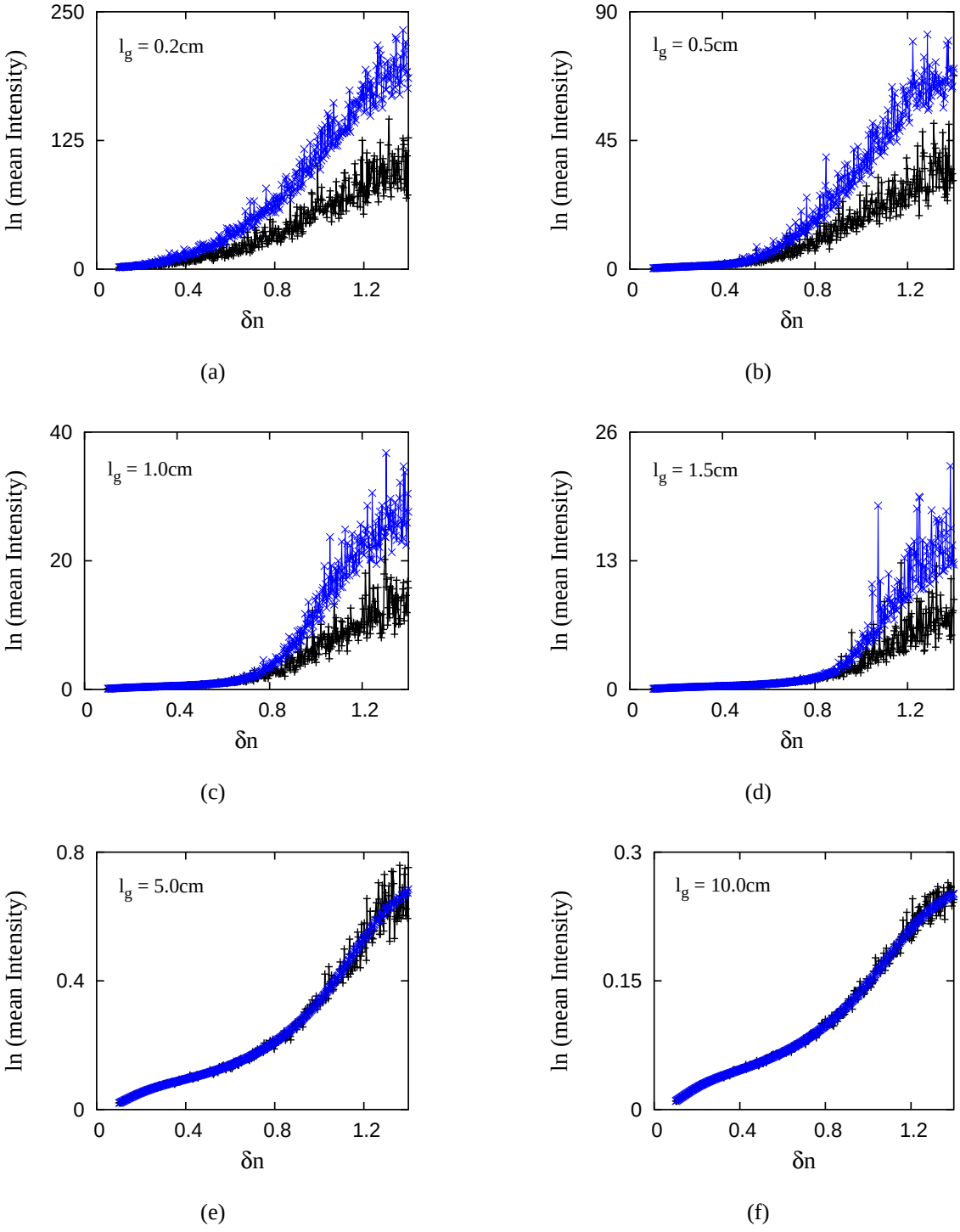

Figure 3.4: *Mean intensity (log scale) as function of δn for various l_g with scatterer size = 0.38 μm; "+" (black): 1,000 simulation runs and "× (blue)" : 1000,000 simulation runs.*

fluctuations at high gains which become operative at these strong scatterings. On the other hand, the smooth mean emission intensity profiles observed at low gain or lesser scattering strength indicates the crossover to the Gaussian statistics. The increase in means is indicative of the tendency of divergence of mean at high gains and strong scatterings.

Another interesting feature seen is the geometrical effect or structural resonances. Figures 3.5(a) and 3.5(b) show the mean intensity as function of δn and the best fits for $l_g = 0.5$ cm and $l_g = 10.0$ cm respectively ($d = 0.38\ \mu$m, $n_s = 10^{10}$/cc, and $\lambda = 0.633\ \mu$m). Figures 3.5(c) and 3.5(d) give the deviation (ΔI) of the mean intensity from their respective best fits as function of δn for $l_g = 0.5$ cm and $l_g = 10.0$ cm respectively. Interestingly, a near periodic oscillation about the best fit is observed as a dominant feature at low gain and low scattering (Fig. 3.5(d)). We attribute this to geometrical effects, namely the change in wavelength within the scatterer ($\delta\lambda$) associated with the change in refractive index mismatch (δn) is comparable with the circumference of the scatterer (the Mie resonant condition).
Here : $\pi d \approx \delta\lambda = \lambda/\delta n$, where, $d = 0.38\ \mu$m, $\lambda = 0.633\mu$m and $\delta n = 0.5$.
Resonance occurs periodically. At high gains, the large Lévy fluctuations mask the geometrical variation (Fig. 3.5 (c)). Similar features were observed for smaller scatterer sizes of $0.26\ \mu$m and $0.18\ \mu$m.

We now examine quantitatively the statistics of the fluctuations observed in the simulations. In the previous chapter, we had shown from theoretical considerations (section 2.2) that for a diffusive RAM composed of point-like scatterers randomly dispersed in an amplifying continuum, the probability distribution for the gain ($p_g(g)$) acquired by a spontaneously emitted diffusively propagating photon, as a result of multiple scattering in the amplifying medium, is given as

$$p_g(g) = \sum_{m=1}^{\infty} \left(\frac{8\pi a \rho_o l_t l_g}{3}\right) \frac{1}{g^{1+\alpha_m}}, \tag{3.7}$$

where, $\alpha_m = m^2(\pi^2 l_t l_g/3a^2)$: the mth Lévy exponent, ρ_o is the initial probability density and a is radius of the RAM. It was argued that the smallest exponent α_1 dominates, and it suffices to consider only the first term. Thus,

$$p_g(g) \simeq \left(\frac{8\pi a \rho_o l_t l_g}{3}\right) \frac{1}{g^{1+\alpha_1}}, \tag{3.8}$$

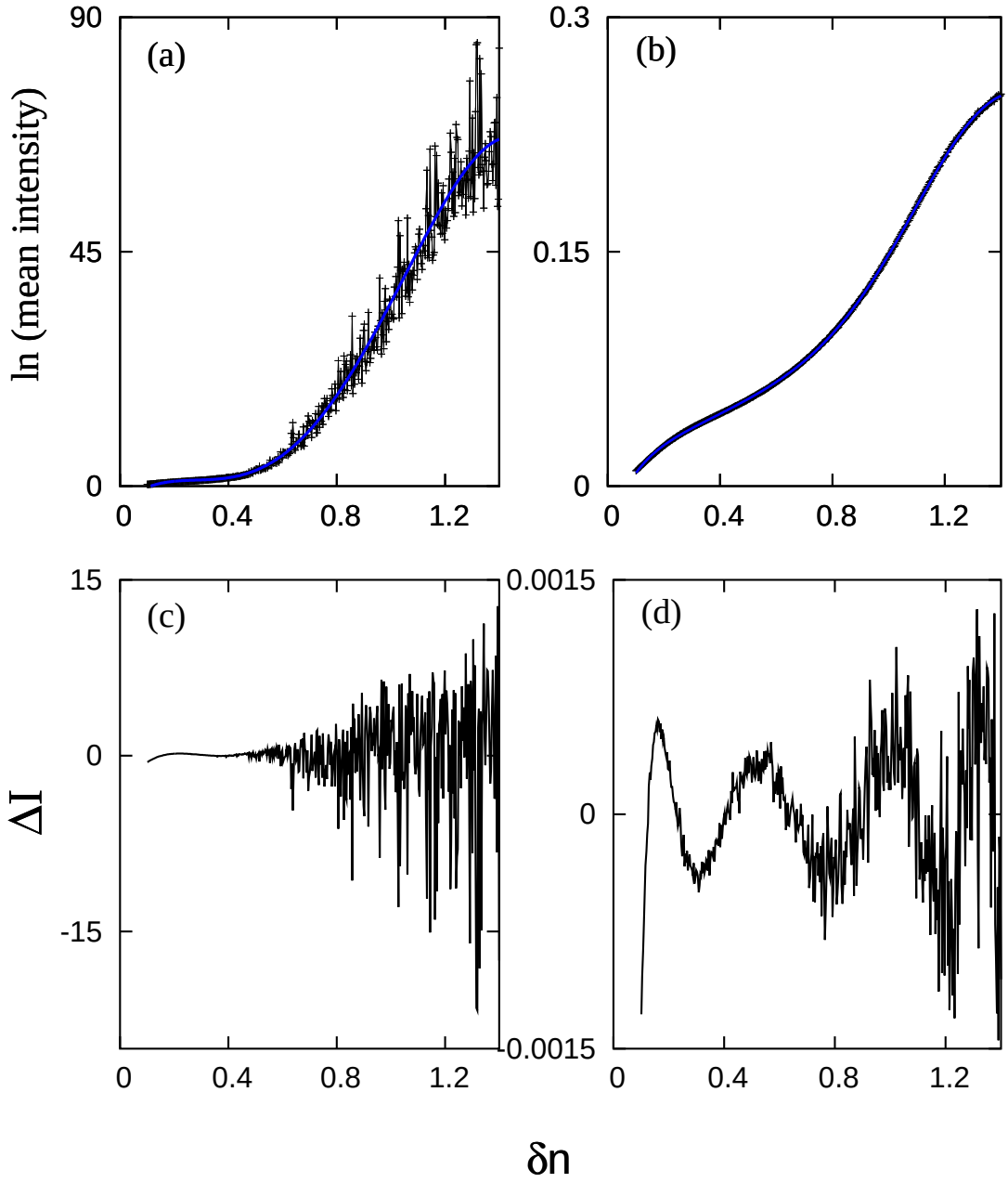

Figure 3.5: *Mean intensity (log scale) as function of refractive index mismatch (δn) and their best fits (blue curves) (a) l_g = 0.5 cm (b) l_g = 10.0 cm. Intensity deviation of the mean intensity from its best fit (ΔI) as function of δn (c) l_g = 0.5 cm (d) l_g = 10 cm. Scatterer size = 0.38 μm*

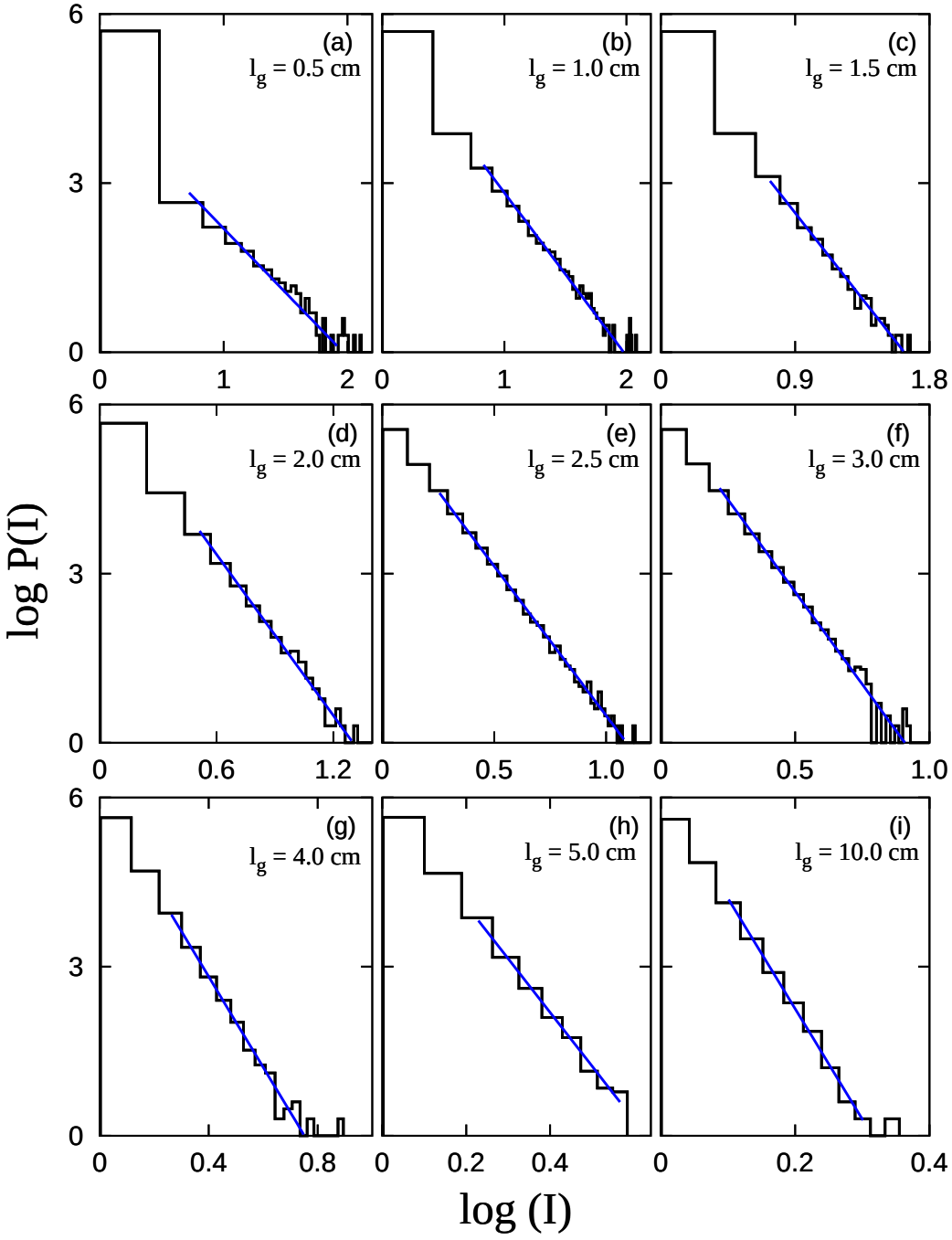

Figure 3.6: *Intensity histograms, log (P(I)) versus log (I), for different l_g with d = 0.26 μm, λ = 0.633 μm, δn = 0.82 (n_{sphere} = 2.7, n_{bulk} = 1.88), $n_s = 10^{10}$/cc. Lévy exponents (α) are : 1.27, 1.90, 2.38, 3.76, 4.30, 5.55, 7.03, 8.54 and 18.59 for (a) to (i) respectively, obtained from straight line fits (blue).*

where, $\alpha_1 = \pi^2(l_t l_g/3a^2)$. Henceforth, in rest of the Thesis, we use α to denote the first Lévy exponent (α_1).

Next, from the 500,000 intensity values obtained for a given set of RAM parameters namely, the intensity histograms (log-log scale) were constructed by plotting the number of times an intensity value occurs (probability P(I)), as function of the intensity (I). As suggested by Eq. 3.14, these intensity histograms (log-log scale) are expected to give straight line fits with negative slopes ($1 + \alpha_1$), from which we calculate the Lévy exponent (α_1).

We first constructed the intensity histograms (log-log scale) as function of gain (l_g^{-1}). Figures 3.6(a)-(i) give the intensity histograms for different gain lengths (l_g) with the RAM parameters : $d = 0.26\ \mu$m, $n_s = 10^{10}$/cc, $\delta n = 0.82$ and $\lambda = 0.633\ \mu$m. These, indeed, give straight line fits with the slope decreasing with decreasing l_g (increasing gain). Note that the decreasing slope implies a smaller α and hence, a more pronounced Lévy feature. In particular, the Lévy exponents are calculated to be 18.59, 8.54, 7.03, 5.55, 4.30, 3.76, 2.38, 1.90 and 1.27 for l_g = 10.0 cm, 5.0 cm, 4.0 cm, 3.0 cm, 2.5 cm, 2.0 cm, 1.5 cm, 1.0 cm and 0.5 cm respectively. Thus, a crossover from the Gaussian ($\alpha \geq 2$) to the Lévy ($\alpha < 2$) statistics is seen as l_g is decreased from 10.0 cm (Fig. 3.6(i)) to 0.5 cm (Fig. 3.6(a)).

Figure 3.7(a) shows the Lévy exponent (α) plotted as function of l_g. Clearly, α varies linearly with l_g (as predicted by our theoretical analysis, Eq 2.24).

To examine the effect of increased scattering strength in RAM, intensity histograms were plotted (Fig. 3.8) for different l_g, with the scatterer size increased to 0.30 μm (keeping the other RAM parameters the same as in Fig. 3.6). Straight line fits to these intensity histograms yield the Lévy exponents (α) of 14.36, 7.59, 5.65, 4.23, 3.57, 2.85, 2.06, 1.37 and 0.61 for l_g = 10.0 cm, 5.0 cm, 4.0 cm, 3.0 cm, 2.5 cm, 2.0 cm, 1.5 cm, 1.0 cm and 0.5 cm respectively. The Lévy exponents (α) are clearly seen to vary linearly with l_g (Fig. 3.7(b)).

On comparing the relative values of α as function of l_g, in Figures 3.7(a) and 3.7(b), we notice that the RAM having larger scatterer size (greater scattering strength) exhibits lower Lévy exponents or more pronounced Lévy features.

Next, we plotted the intensity histograms (log-log scale) for different scatterer sizes (which effectively correspond to different transport mean free path lengths l_t). As was dis-

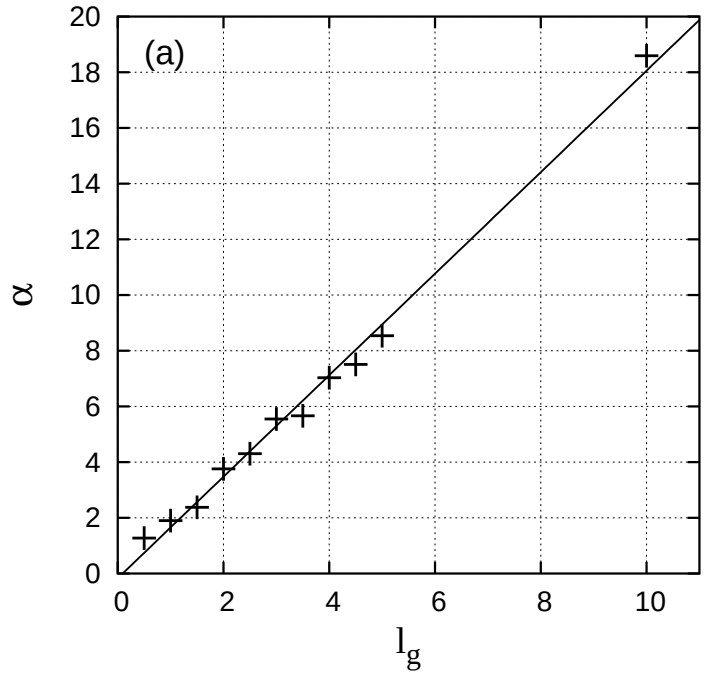

(a)

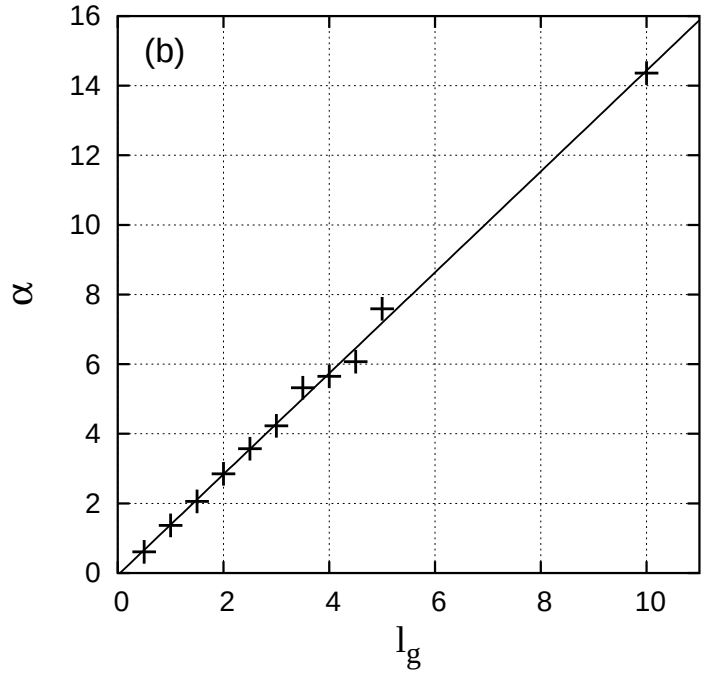

(b)

Figure 3.7: *Lévy exponent α as a function of gain length (l_g) with $\delta n = 0.82$ ($n_{sphere} = 2.7$, $n_{med} = 1.88$) for scatterer size (a) 0.26 μm, (b) 0.30 μm. Straight line fits are also shown.*

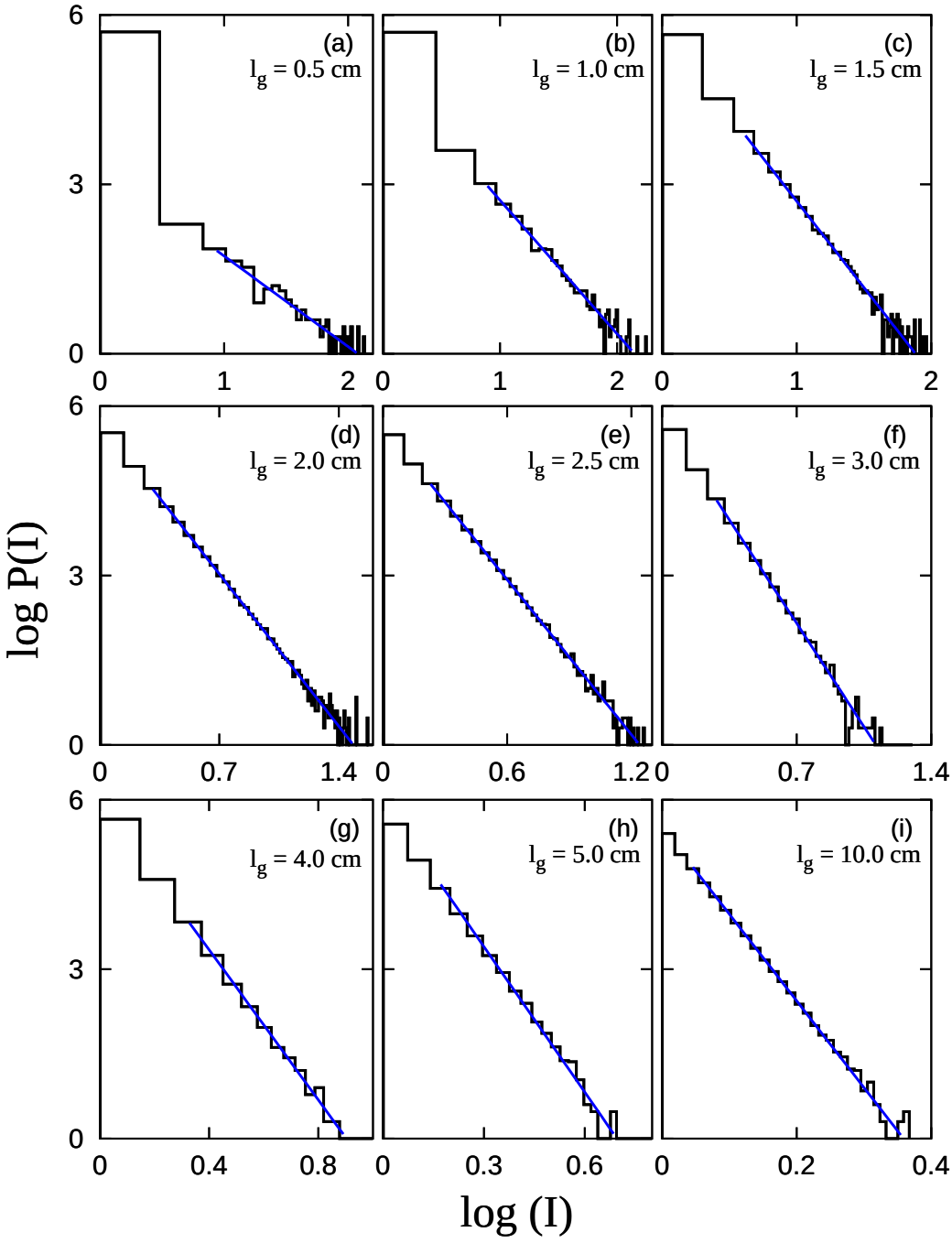

Figure 3.8: *Intensity histograms, log (P(I)) versus log (I), for different l_g with d = 0.30 μm, λ = 0.633 μm, δn = 0.82 (n_{sphere} = 2.7, n_{bulk} = 1.88), n_s = 10^{10}/cc. Lévy exponents (α) are : 0.61, 1.37, 2.06, 2.85, 3.57, 4.23, 5.65, 7.59 and 14.36 for (a) to (i) respectively, obtained from straight line fits (blue).*

cussed in chapter 1, for a given set of RAM parameters (e.g., n_s, λ and δn), an increase in scatterer size increases the scattering cross-section (σ_s) leading to a smaller transport mean free path ($l_t \sim \sigma_s^{-1}$). Figures 3.9(a)-(f) give the intensity histograms (in the log-log scale) and their straight-line fits for different transport mean free path lengths l_t (corresponding to different scatterer sizes) with l_g = 4.0 cm, δn = 0.30, $n_s = 10^{12}$/cc and λ = 0.633 μm.

The figure 3.9, clearly, shows that the slopes of the straight line fits (or the Lévy exponents α) decrease with the decrease in l_t (or increase in scattering strength corresponding to increased scatterer size). The Lévy exponents are found to be 3.67, 1.85, 1.16, 0.93, 0.72 and 0.55 for l_t = 0.117 cm, 0.058 cm, 0.035 cm, 0.025 cm, 0.018 cm, and 0.013 cm respectively (corresponding to scatterer sizes of 0.18 μm, 0.22 μm, 0.26 μm, 0.30 μm, 0.34 μm, and 0.38 μm respectively). Thus, a crossover from the Gaussian ($\alpha \geq 2$) to the Lévy ($\alpha < 2$) statistics is observed on decreasing l_t (or increasing scattering by increasing the scatterer size). Figure 3.10(a) clearly shows a linear variation of α with l_t (as predicted by our theoretical analysis, Eq 2.24).

Figure 3.11(a)-(f) shows the intensity histograms (in log-log scale) and their straight line fits for different l_t (corresponding to different scatterer sizes) with the refractive index mismatch (δn) increased to 1.02 (while keeping the other RAM parameters the same as in Fig. 3.9). Once again, a crossover from the Gaussian to the Lévy statistics was observed with the Lévy exponents α = 3.00, 1.66, 1.09, 0.93, 0.78 and 0.72 for l_t = 0.74 cm, 0.29 cm, 0.17 cm, 0.12 cm, 0.09 cm, and 0.06 cm respectively (corresponding to scatterer sizes of 0.18 μm, 0.22 μm, 0.26 μm, 0.30 μm, 0.34 μm, and 0.38 μm respectively). As is expected, the RAM characterized by higher mismatch (which effectively corresponds to increased scattering strength) gives lower Lévy exponents as function of l_t. Figure 3.10(b) shows the linear variation of α with l_t.

These results (for a wide range of d, δn, n_s and l_g), thus, clearly show that a crossover from the Gaussian to the Lévy statistics can be achieved either by increasing the gain (l_g^{-1}) or by increasing the scattering strength (by δn, d and n_s) in the RAM. In fact, the absolute values of δn, d, n_s and l_g, provide a complete control over the Lévy exponents (α). Further, the simulations verified our theoretical prediction (discussed in section 2.2) of the linear

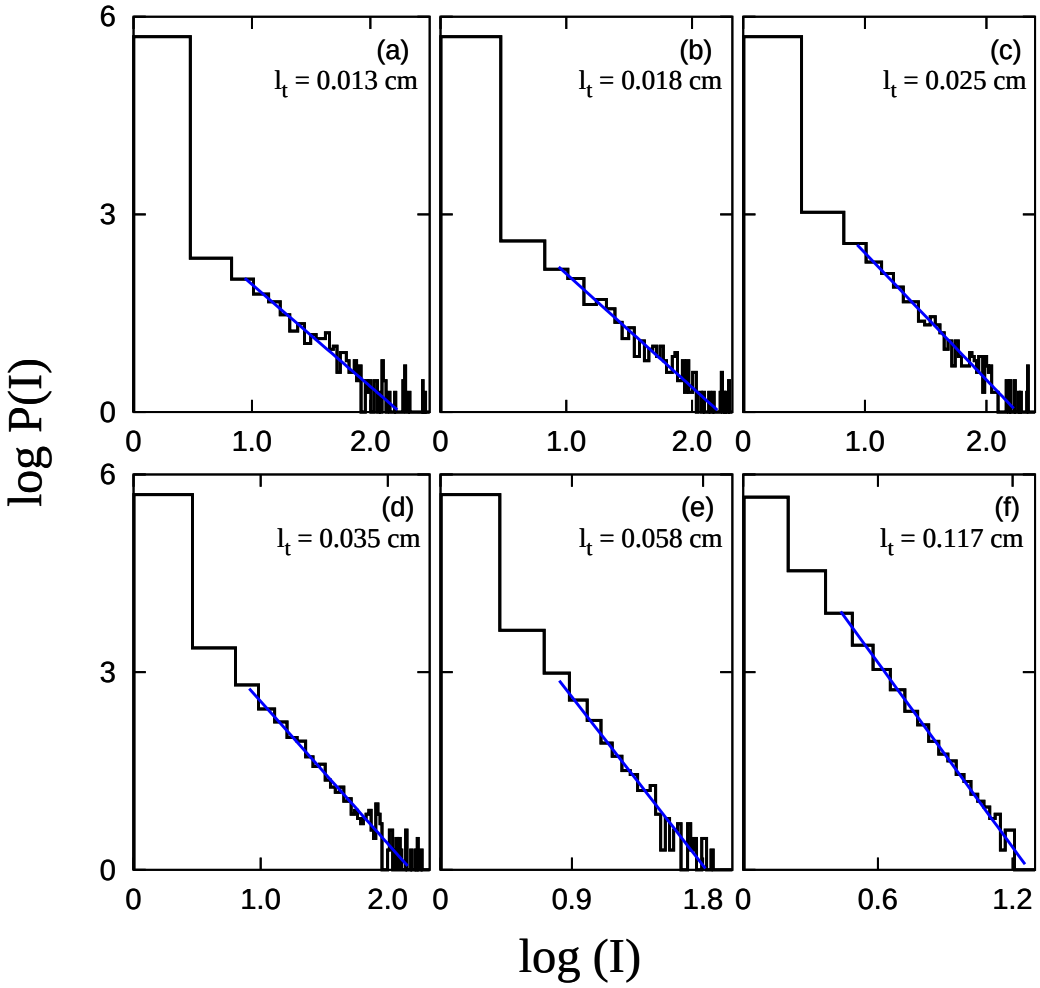

Figure 3.9: *Intensity histograms, log (P(I)) versus log (I), for different l_t, corresponding to different scatterer sizes, with l_g = 4.0 cm, δn = 0.3 (n_{sphere} = 2.7, n_{bulk} = 2.4), λ = 0.633 μm, $n_s = 10^{12}$/cc. Lévy exponents (α) are : 0.55, 0.72, 0.93, 1.16, 1.85 and 3.67 for (a) to (f) respectively, obtained from straight line fits (blue).*

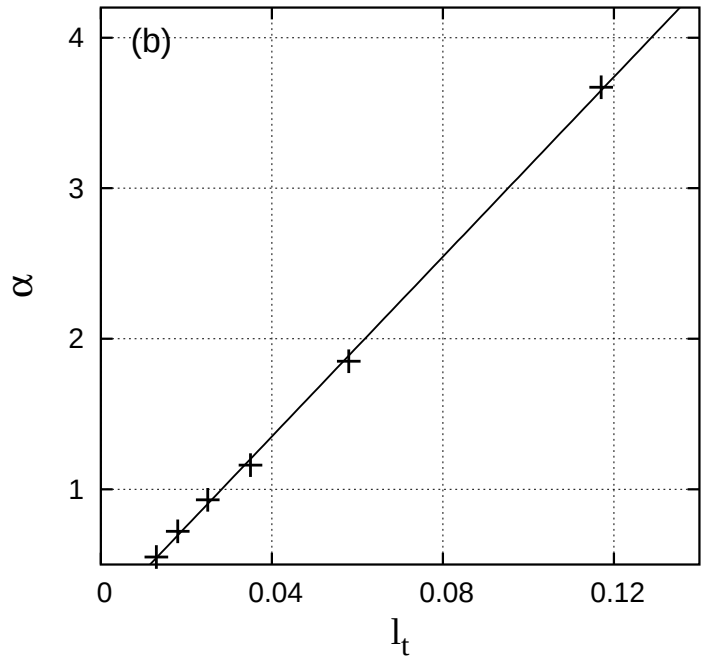

(a)

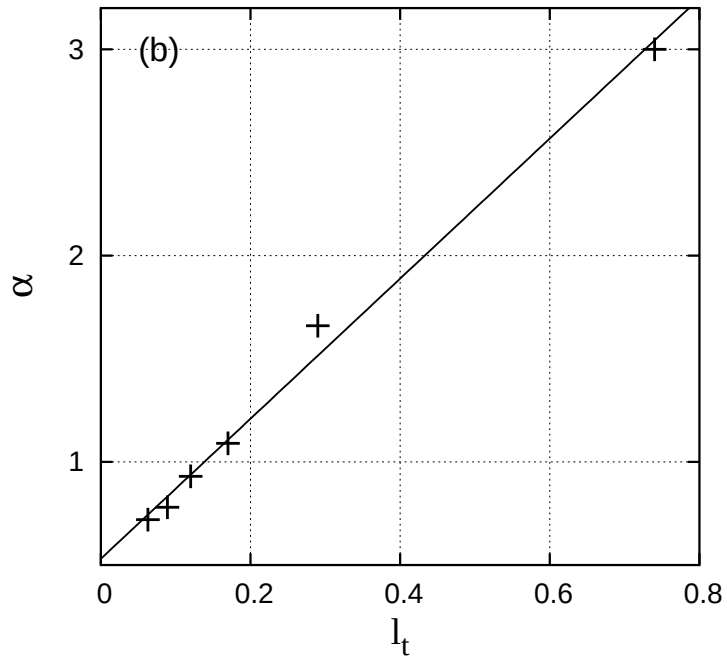

(b)

Figure 3.10: *Lévy exponent α as a function of transport mean free path (l_t) with l_g = 1.0 cm for δn (a) 0.3 (n_{sphere} = 2.7, n_{med} = 2.4), (b) 1.02 (n_{sphere} = 2.7, n_{med} = 1.68). Straight line fits are also shown.*

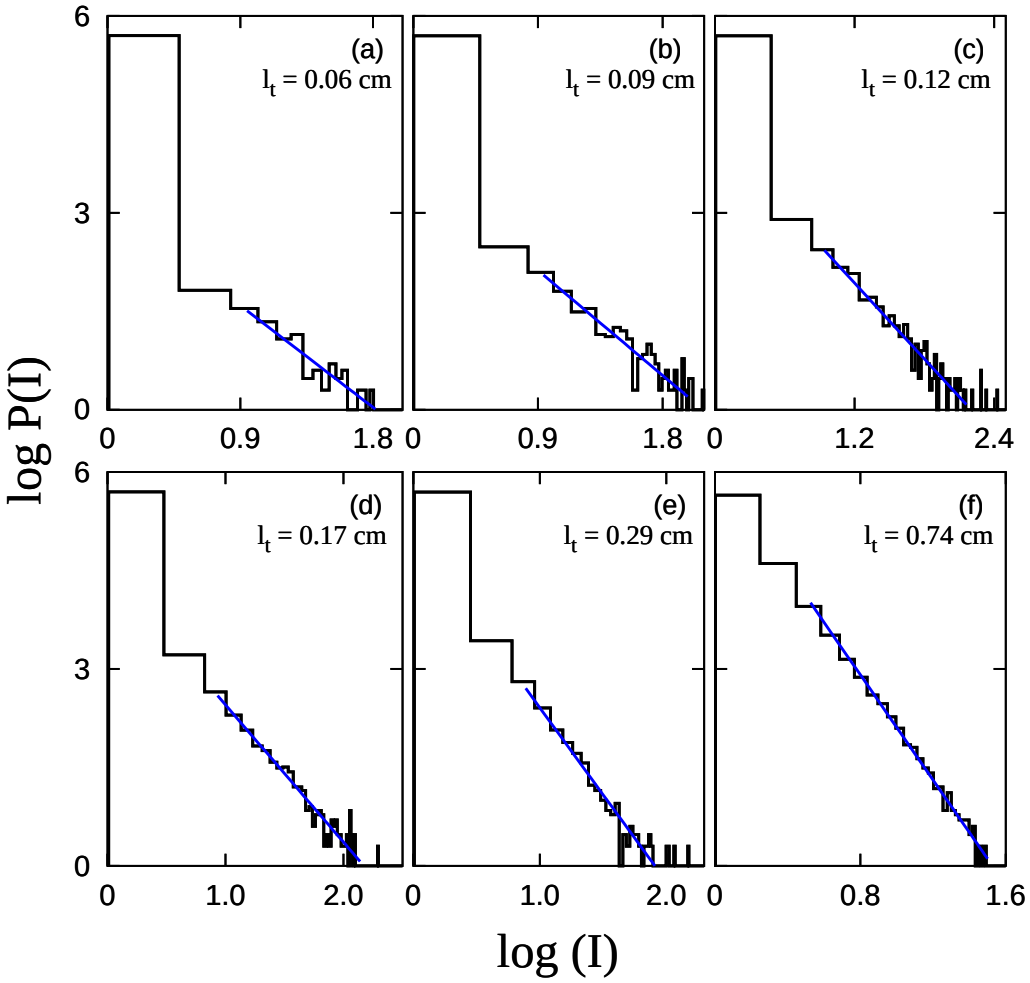

Figure 3.11: *Intensity histograms, log (P(I)) versus log (I), for different l_t (corresponding to different scatterer sizes) with l_g = 1.0 cm, δn = 1.02 (n_{sphere} = 2.7, n_{bulk} = 1.68), λ = 0.633 μm, $n_s = 10^{10}$/cc. Lévy exponents (α) are : 0.72, 0.78, 0.93, 1.09, 1.66 and 3.00 for (a) to (f) respectively, obtained from straight line fits (blue).*

dependence of α on l_t and l_g.

It may be noted that, though, we have presented results of Monte Carlo simulations over 500,000 photon paths, the simulations were also performed for twice (i.e., 1×10^6) and ten times (i.e., 5×10^6) that number of photon paths (simulation runs). The results, in particular the Lévy exponents (α) obtained from the intensity histograms, remained the same (Fig. 3.12).

So far we have focussed on the statistics of intensity fluctuations over different realizations of randomness (in the present case, different simulation runs) bringing out their Lévy-statistical feature ($\alpha < 2$), where the second moment diverges[2]. We now turn to yet another rather interesting statistical aspect of our simulations that has to do with the so called Lévy microscope effect [5] (where an extremely large but extremely improbable/rare event dominates the given series of events), that should obtain in the limit of very high gain corresponding to the Lévy exponent ($\alpha < 1$) when the mean intensity itself diverges . To recall, for $1 < \alpha < 2$, while the variance diverges, the mean is finite. On the other hand, for $\alpha < 1$, both the mean and the variance diverge. Here, the sum over intensities is seen to be dominated by the largest typical intensity value or a few values. In order to capture this effect, we considered a sequence of N successive simulation runs (realization of photon paths) for very large N (e.g., 500,000). It is convenient to introduce here nested subsequences in which the i^{th} subsequence comprises the first N_i simulation runs with $N_1 < N_2 < N_3 .... N_i < N_{i+1} .... <= N$. In particular, $N_{i+1} = N_i + \Delta N$, with N_i varied from 10 to 500,000 in steps of 10. We defined the corresponding (i^{th}) subsequences's average intensity as the total emission intensity obtained for the first N_i simulation runs, divided by N_i. We then plotted (I_i) versus (N_i) (on the log-log scale) for certain choice of the RAM parameters for very high gain and strong scattering, i.e. when the exponent $\alpha < 1$. This is shown in Fig. 3.13 with the following choice of parameters : $N = 500,000$, $l_g = 0.2$ cm, $d = 0.38$ μm and $\delta n = 1.14$. The large jumps seen in the plot (curve a) are a signature of a Lévy microscope, namely, the dominance of sum of intensities by the typical largest (single or a few) intensity value(s). We have also shown, for comparison, the Gaussian case of low gain and weak scattering (curve b), with the RAM parameters

[2]Interestingly, the threshold condition for diffusive lasing, first obtained by Letokhov [4], corresponds to this limit (discussed in chapter 2, section 2.2).

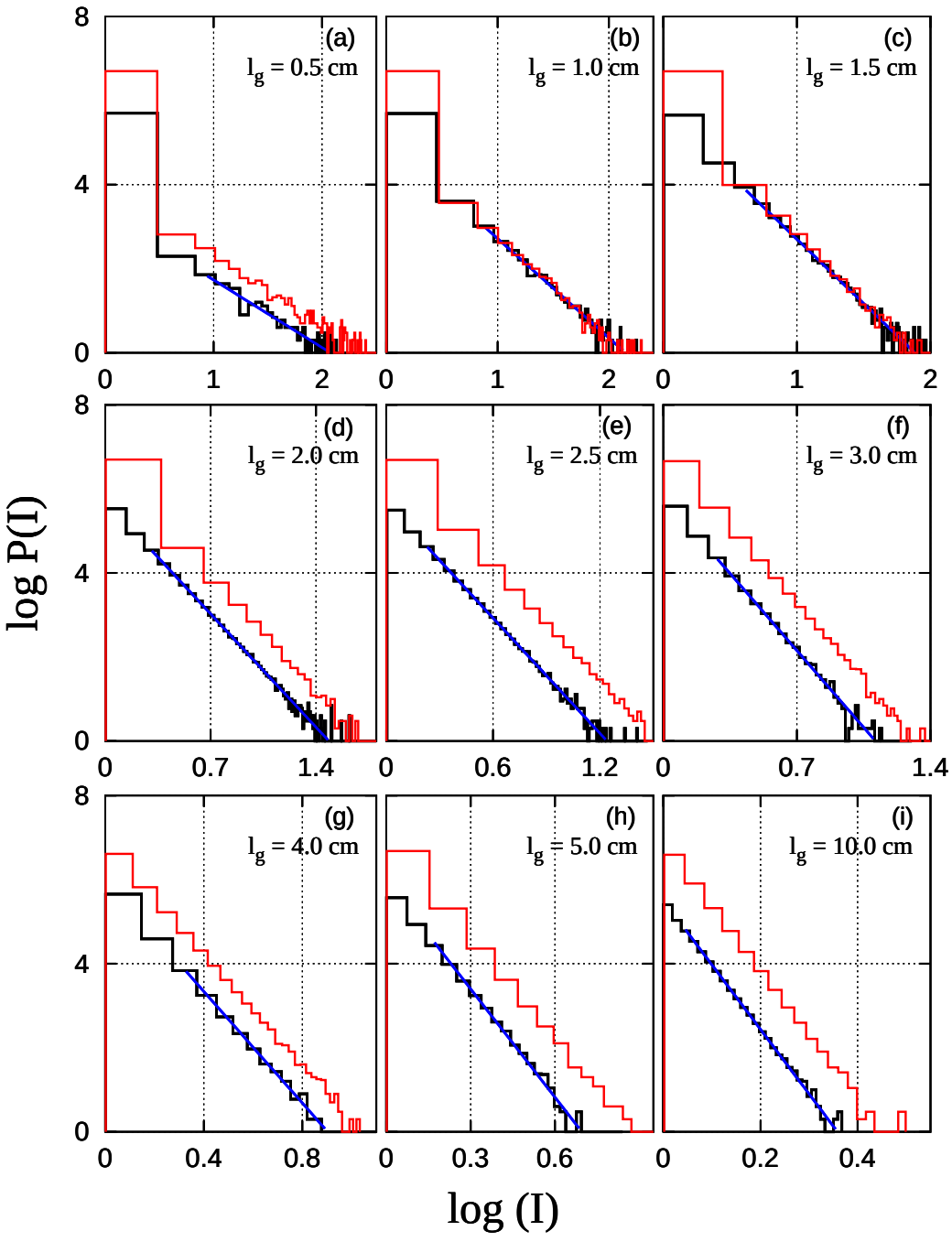

Figure 3.12: *Intensity histograms, log (P(I)) versus log (I), for different* l_g*. Each subfigure contains two intensity histograms corresponding to* 5×10^5 *(black) and* 5×10^6 *(red) simulation runs. Straight line fits (blue) are also shown for the former.*

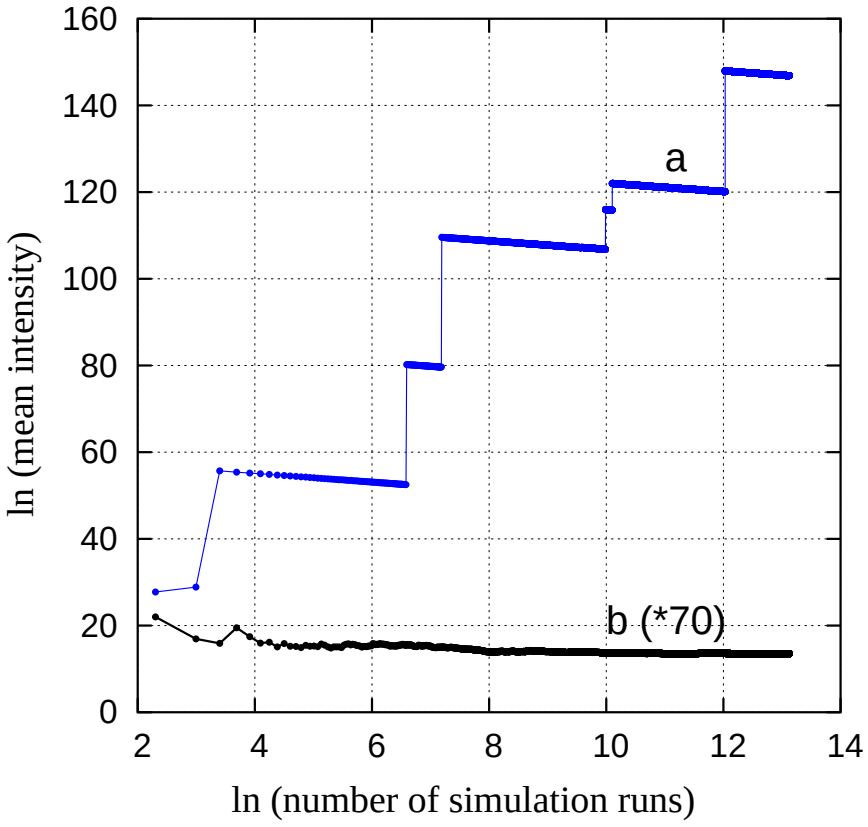

Figure 3.13: *Log-log scale plot of mean intensity (I_i) versus size of subsequence (N_i). RAM parameters are : (a) l_g = 0.2 cm (blue); (b) l_g = 10 cm (black), with d = 0.38 μm and δn = 1.14. Note that curve (b) has been multiplied by a factor of 70 to bring it to the same scale as (a).*

: $N = 500,000$, $l_g = 10$ cm, $d = 0.38$ μm and $\delta n = 1.14$. The featureless, essentially flat curve, devoid of large intensity jumps, is in sharp contrast to the Lévy case and confirms that the Lévy microscope effect can be observed only at very high gain (l_g^{-1}) and strong scattering (l_t^{-1}).

3.4 Conclusions

In conclusion, the results of our Monte Carlo simulations of photon diffusion through a RAM (dye-scatterer system) show that the mean emission intensity increases with the increase

in scattering strength and gain. Further, we found that the non-monotonic increase in the mean intensity as function of refractive index mismatch in the limit of high gain and strong scattering can be associated with the Lévy statistical features. On the other hand, the smooth intensity profile at low gain and less scattering is a signature of the Gaussian statistics. Our simulations demonstrated a crossover from the Gaussian to the Lévy statistics as function of scattering strength (l_t^{-1}; via scatterer size d, refractive index mismatch δn, and scatterer density n_s) and gain (l_g^{-1}). These results are in agreement with our earlier model calculation and physical experiments (discussed in chapter 2). In addition, our simulations also reveal the so called Lévy microscope effect in the limit of very high gain and strong scattering where the mean intensity is dominated by a single largest event. Finally, we note that our simulations allow us to explore the parameter regime (of very high gain and strong scattering) which is not readily accessible in physical experiments.

We would like to point out that the simulation at present does indeed assume uniform pumping, though it is straightforward to incorporate non-uniform pumping by considering the value of l_g dependent on coordinates. However, the emphasis of the work is on studying the crossover from the Gaussian to the Lévy statistics of fluctuations in the emission intensity from the RAM for the simplest model. Hence the idealization. Further, our simulation is idealized in that it does not take into account the nonlinear effects, e.g., gain saturation.

Bibliography

[1] C.F. Bohren and D.R. Huffman, *Absorption and Scattering of light by small particles*, (Wiley, New York, 1983).

[2] L.C. Henyey and J.L. Greenstein, Astrophys. J. 93 (1941) 70.

[3] M. Romeo, V. Da Costa and F. Bardou, Eur. Phys. J. B **32**, 513 (2003).

[4] V.S. Letokhov, Sov. Phy. JETP **26**, 835-840 (1968).

[5] F. Bardou, arXiv:physics/ 0012049 v1, 20 Dec 2000.